Epitaxial Crystallization of Precisely Methyl-Substituted Polyethylene Induced by Carbon Nanotubes and Graphene

Weijun Miao [1], Yiguo Li [2] , Libin Jiang [1], Feng Wu [1], Hao Zhu [1], Hongbing Chen [1] and Zongbao Wang [1,*]

[1] Ningbo Key Laboratory of Specialty Polymers, Faculty of Materials Science and Chemical Engineering, Ningbo University, Ningbo 315211, China; 15988621876@163.com (W.M.); 18892615669@163.com (L.J.); 18892615653@163.com (F.W.); zh2320015@163.com (H.Z.); chenhongbing@nbu.edu.cn (H.C.)

[2] Anhui Collaborative Innovation Center for Petrochemical New Materials, School of Chemistry and Chemical Engineering, Anqing Normal University, Anqing 246011, China; liyiguo@aqnu.edu.cn

* Correspondence: wangzongbao@nbu.edu.cn

Abstract: How large of a substituent/branch a polyethylene possesses that can still be induced by nanofillers to form ordered chain structures is interesting, but uncertain. To solve this problem, precisely methyl-substituted polyethylene (PE21M) was chosen as a model to prepare its one-dimensional and two-dimensional nanocomposites with carbon nanotubes (CNTs) and graphene via solution crystallization. It is shown that kebab-like and rod-like nanofiller-induced crystals were separately observed on the surfaces of CNTs and graphene and the density of rod-like crystals is significantly less than kebab-like ones. The results of differential scanning calorimetry (DSC) and X-ray diffraction (XRD) reveal that CNTs and graphene cannot induce polymers with the substituent volume greater than, or equal to, 2 Å (methyl) to form ordered lattice structure, but CNTs exhibit the better nucleation effect, providing us with guidance to manipulate the physical performance of polymer composites on the basis of the size of the substituent and the type of nanofiller.

Keywords: PE21M; carbonaceous nanofiller; epitaxial crystallization

1. Introduction

Epitaxial crystallization of semi-crystalline polymers on foreign surfaces can produce controllable crystal structures and morphologies which, therefore, provides an efficient way to tailor the physical performance of polymeric materials [1–4]. It is widely recognized that the mechanism of epitaxial crystallization is based on some certain crystallographic matches [1], and the mismatching of the contact lattice planes between the substrate and polymers cannot exceed 15%. For example; one-dimensional or two-dimensional lattice matches generate special interactions between the polymer chains and the substrate in the contacting interface which can alter not only the crystal structure and morphology of polymers, but the crystallization kinetics [2–6]. One-dimensional carbon nanotubes (CNTs) and two-dimensional graphene are frequently used as substrates to induce polymer crystallization because of their high surface area. It has been well documented that the topological structure of substrates has a significant influence on the polymer crystallization behavior [7–15]. Generally, the mechanism of CNTs inducing polymers to form disk-like crystal lamellae was described as "soft epitaxy" [16–18]. While, for two-dimensional graphene, lattice matching should play the dominant role in surface-induced polymer epitaxial crystallization [19–22]

Polyethylene is one of the most studied polymers due to its versatility in a very wide range of applications. The common method for modifying the structures and properties of polyethylene is

randomly copolymerizing ethylene with 1-alkene or with polar/nonpolar comonomers. However, random copolymerization leads to the products with a bivariate comonomer content-molar mass distribution, so the physical properties can vary depending on the molecular weight, molecular-weight distribution, branch identity, branch content, and branch distribution, and are also difficult to reproduce at a high level of consistency [23,24]. Accordingly, the relationship between the structure and performance of random copolyethylene is quite ambiguous. Polymers synthesized by acyclic diene metathesis polymerization (ADMET) offer the suitable model systems to study the relationship of the structure and performance which possess a well-defined primary structure. ADMET polymers have a general repeating unit, $-[(CH_2)_m\text{-}CHX]_n-$, where m is in the range of 8–74 and X is the group of various types placed at a precise distance along the PE backbone, such as halogen, alkyl group, or other functional groups [25–33]. These polymers were found to show the various crystalline phases depending on the side group X. Meanwhile, the aggregation state of precision macromolecules may be affected remarkably by a small change of the chain structure and the distribution of defects in crystallites can be exquisitely controlled by the crystallization kinetic, which is not yet feasible in classical branched polyethylene obtained via coordination catalysis [34,35]. In our previous works, the precise ADMET polyethylene with halogen atoms (F, Cl, Br) placed on each every 21st backbone carbon were chosen as models to investigate the structural change of polymer epitaxial crystallization. The results demonstrated that CNTs had almost no affection on the structure of PE21F and PE21Cl, but RGO induced the structural transformation of PE21Cl and PE21Br from a triclinic form to orthorhombic form, which generated extraordinarily high melting temperatures [36–38]. Such a significant change of the crystal structure resulting from surface induced epitaxial crystallization not only suggests that the precisely substituted polyethylenes are ideal models to explore the influence of the substituent on epitaxial crystallization, but also indicates that single-walled carbon nanotubes (SWCNTs) and reduced graphene oxide (RGO) possess different capacities to induce substituted polymers to generate ordered chain packing structures due to the different epitaxy mechanism of the two nanofillers. However, how large of a substituent/branch a polyethylene possesses that can still be induced by nanofillers to form ordered chain structures is unknown.

For solving this question, in this paper, the precision ADMET polyethylene with the methyl placed on every 21st backbone carbon (PE21M) was chosen as a model to investigate the epitaxial crystallization of polymer with a much bulkier substituent. The larger volume of methyl (2.0 Å) compared to those of F (1.47 Å) to Cl (1.75 Å) and Br (1.85 Å) results in a much more disordered crystal lattice and the lower melting temperature of PE21M, and the bulkier substituent is beneficial for exploring the capacities of carbonaceous nanofillers that have different mechanisms of epitaxial crystallization to induce nucleation and crystallization of substituted/branched polymers. Meanwhile, one-dimensional SWCNTs and two-dimensional RGO were employed as nanofillers to prepare PE21M-based nanocomposites and the epitaxial crystallization of nanocomposites was achieved via solution crystallization. The resultant crystal morphology and structures were analyzed by transmission electron microscopy (TEM) and X-ray diffraction (XRD) and the thermal behaviors were characterized by differential scanning calorimetry (DSC). Finally, the discrepancy of the density of crystals formed on two nanofillers was also discussed to compare their epitaxy ability. This study is expected to enhance the understanding of the influence of low-dimension carbonaceous nanofillers on the nucleation and chain packing structure of semi-crystalline polymers with large substituents/branches.

2. Experimental Section

2.1. Materials

Purified HiPco single-walled CNTs (SWCNTs, with an average diameter of 6 nm) were purchased from Times Nanotechnologies Inc (Chengdu Organic Chemicals Co. Ltd., Chengdu, China) and used as received. Reduced graphene oxide (RGO) was prepared by thermal exfoliation and reduction of

graphene oxide (GO) [39]. The precisely substituted polyethylene with methyl placed on each every 21st backbone carbon has been studied, labelled as PE21M, where the number corresponds to the precise location of the side group in the PE backbone. The synthesis route of PE21M is shown in Scheme 1 [31]. The chemical structure was characterized by ^{1}H NMR (Supporting Information Figure S1). The molecular weight was determined by gel permeation chromatography (GPC) using an Agilent PL-GPC 220 instrument with HPLC-grade chloroform as the mobile phase at a flow rate of 1.0 mL·min^{-1} and a calibration with polystyrene standards (M_n = 12,962 g/mol, M_w/M_n = 2.17).
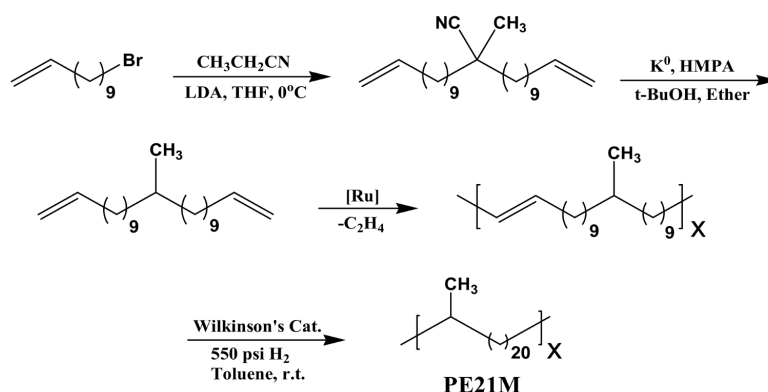
Scheme 1. Monomer and polymer synthesis process.

2.2. Sample Preparation

The fabrication of PE21M nanocomposites were described as follows. The nanofiller/*p*-xylene mixed solution with the nanofiller mass concentration of 0.1 wt % was sonicated for 2–3 h at 45 °C and the PE21M/*p*-xylene mixed solution with PE21M mass concentration of 0.1 wt % was prepared by dissolving PE21M into *p*-xylene at 120 °C for 2 h. Then, 10 g nanofillers/*p*-xylene solution was mixed with 10 g PE21M/*p*-xylene solution at 120 °C for 5 min. The mixture was finally quenched to the preset crystallization temperature, T$_c$. In order to avoid SWCNTs to agglomerate and form small bundles in solvent, the mixed solution was stirred at 1200 r·min^{-1}. The sample was isothermally filtered after crystallization for 6 h. After washing with ethanol carefully three times, nanocomposites were dried at 40 °C under vacuum for 36–48 h.

Furthermore, Qunxu's method [40] was employed to prepare PE nanocomposites by supercritical CO_2 (SC CO_2). The mixture of nanofiller/*p*-xylene solution and PE21M/*p*-xylene solution was produced by the same procedure above-mentioned. Then the mixture was quickly transferred into a stainless steel autoclave at the preset crystallization temperature T$_c$. SC CO_2 was then charged into the autoclave up to the desired pressure within a short time. After maintaining the supercritical fluid condition for 3 h, the system was slowly depressurized and the sample was collected and labelled.

2.3. Characterization

Nanocomposite suspensions were collected on a carbon-coated grid. The crystal morphology observation was conducted by a JEOL JEM2100 transmission electron microscope (TEM, JEOL., Tokyo, Japan) with an accelerating voltage of 200 kV. Differential scanning calorimetry (DSC) experiments were carried out using a Perkin-Elmer DSC8000 (PerkinElmer, New York, NY, USA). The samples with an average weight of 2~4 mg were heated from 30 to 100 °C at a scanning rate of 10 °C·min^{-1} under a nitrogen atmosphere. X-ray diffraction (XRD) patterns were recorded on a Bruker D8 diffractometer (Bruker, Karlsruhe, Germany), using Ni-filtered Cu Kα radiation at 40 kV and 30 mA at room temperature at an angle ranging from 5 to 40° at a rate of 3.5°·min^{-1}.

3. Results and Discussion

3.1. Morphologies of PE21M/Nanofiller Composites

3.1.1. Morphologies of PE21M/CNT Kebab-Like Crystals

As expected, the shish-kebab structures periodically form on SWCNTs at all selected experimental temperature, as exhibited in Figure 1 and the average sizes of PE21M lamellae attached to SWCNTs are listed in Table 1 on the basis of the measurement of 200 lamellae. The average diameters of the PE21M kebab crystals are about 16.3 ± 1.0, 20.2 ± 1.1, and 18.4 ± 0.9 nm for 40, 50, and 60 °C, respectively. It is evident that the average size of the PE21M kebab crystals first increases then decreases with the increase of crystallization temperature and the largest diameter of kebabs form at 50 °C. This behavior of crystal growth on SWCNTs is similar to the situations reported in PE21F, PE21Cl, and PE21Br crystals [36–38], which is attributed to the competition of nucleation and crystal growth on the CNTs. Meanwhile, stable crystal nuclei become fewer and fewer with the decrease of undercooling, which can be directly supported by the interval of kebab increasing monotonically with the increase of the crystallization temperature (Table 1). The thickness of the kebab also increases with the crystallization temperature, from 5.1 ± 0.3 nm at 40 °C to 5.6 ± 0.4 nm at 60 °C (Table 1), suggesting that the crystallization ethylene sequence is strongly dependent on the crystallization temperature. We can now conclude that the crystallization temperature has an important influence on the size and periodicity of the shish-kebab structure and the most suitable crystallization temperature for PE21M/SWCNT in *p*-xylene is 50 °C. Our previous studies displayed that the diameter of the PE21F kebab (54–65 nm) was smaller than that of HDPE (50–80 nm) because of the influence of substituent F [36] and the diameter of the kebab decreased rapidly from PE21F (54–65 nm) to PE21Cl (26.2 ± 1.0 nm) and PE21Br (23.2 ± 1.2 nm) with increasing substituent volume (the van der Waals radii of F, Cl, and Br are 1.47, 1.75, and 1.85 Å, respectively) [36–38]. When the van der Waals volume of the substituent increases to 2.0 Å, the diameter of the PE21M kebab decreases to 20.2 ± 1.1 nm (Table 1). The above results further confirm that the substituents act as defects in the chain which have a strong impact on the lateral growth of crystal lamellae. On the other hand, the maximum thickness of PE21M kebabs is 5.6 ± 0.4 nm, which is also the smallest compared to that of PE21F (6.4–8.6 nm), PE21Cl (6.4 ± 0.5 nm), and PE21Br (6.8 ± 0.5 nm) [36–38], further indicating that the crystallization of PE is disturbed more intensely by the larger substituent. By contrasting with our previous works, we found that the interval of PE21M kebab crystals prepared under the same supercooling degree decreases severely with the increase of the substituent's volume [36–38]. The largest interval of PE21M kebab crystals is 20.5 nm, much lower than 48.5 nm of PE21F, 57.7 nm of PE21Cl, and 34.5 nm of PE21Br [36–38]. This can be attributed to the thinner PE21M lamellae resulting in a weak repulsion between adjacent lamellae. According to the "soft epitaxy" mechanism [16–18], CNTs can induce polymers to crystallize regardless of the lattice matching between the polymer chain and the graphitic sheet. Consequently, the density of PE21M crystal nuclei developed on CNTs was almost unaffected by the bulkier substituent.
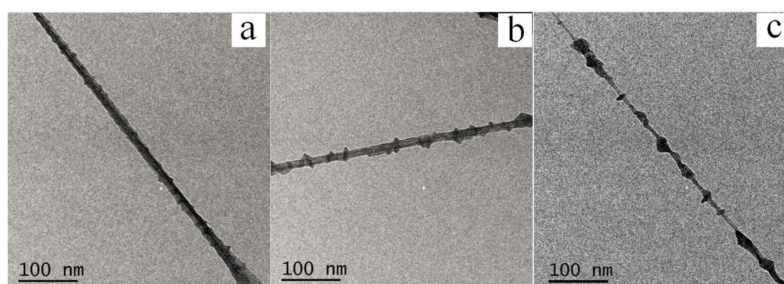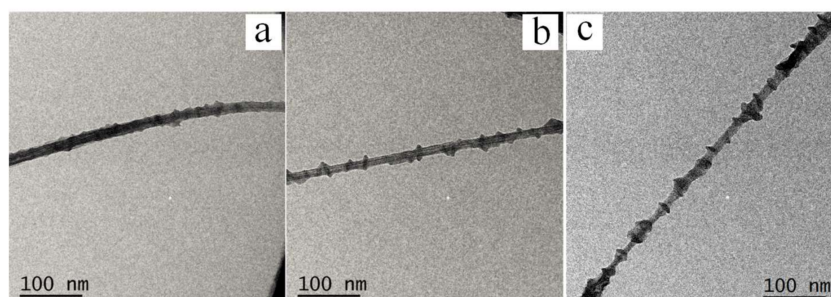

Figure 1. TEM images of PE21M/SWCNT nanocomposites produced in *p*-xylene at different temperatures for 6 h. (**a**) 40 °C, (**b**) 50 °C, (**c**) 60 °C (both PE21Br and SWCNT concentrations are 0.05 wt %).

Table 1. The average size of PE21M lamellae formed on SWCNT based on the TEM images of 200 lamellae.

Sample (Crystallization Temperature)	Diameter of Kebab (nm)	Thickness of Kebab (nm)	Interval of Kebab (nm)
PE21M/SWCNT (40 °C)	16.3 ± 1.0	5.1 ± 0.3	10.0 ± 0.8
PE21M/SWCNT (50 °C)	20.2 ± 1.1	5.4 ± 0.4	16.3 ± 1.0
PE21M/SWCNT (60 °C)	18.4 ± 0.9	5.6 ± 0.4	20.5 ± 1.1

The evolution of kebabs with the isothermal crystallization time was also detected. The morphologies of PE21M crystals on SWCNTs in *p*-xylene at 50 °C for different isothermal crystallization times are shown in Figure 2 and the average sizes of PE21M lamellae are summarized in Table 2. The average diameter of the PE21M kebab crystals is 10.3 ± 0.8 nm after 3 h isothermal crystallization and the continued growth during the subsequent 3 h leads to the diameter of kebabs reaching 20.2 ± 1.1 nm, i.e., the size doubled with respect to the former 3 h. The average growth rate of kebabs is about 3 nm·h^{-1} in the elapsed 6 h, which is far below that of PE21F (20 nm·h^{-1}) [36]. This suggests that the speed of PE21M chain lateral growth is limited by the bulkier substituent. According to the average diameter shown in Table 2, we can find that the diameter of kebab crystals reaches 22.4 ± 0.9 nm after 12 h isothermal crystallization, almost unchanged compared with the isothermal crystallization for 6 h. It can also be observed from Table 2 that little change happens for the thickness and periodicity of kebabs formed at the same crystallization temperatures, which further indicates that the thickness and periodicity of kebabs is directly related to the isothermal crystallization temperatures.

Figure 2. TEM images of PE21M/SWCNT nanocomposites produced by crystallization of PE21M on SWCNTs in *p*-xylene at 50 °C for different isothermal crystallization time. (**a**) 3 h, (**b**) 6 h, and (**c**) 12 h (both PE21Br and SWCNT concentrations are 0.05 wt %).

Table 2. The average size of PE21M lamellae formed on CNTs for different isothermal crystallization time based on the TEM images of 200 lamellae.

Crystallization Time	Diameter of Kebab (nm)	Thickness of Kebab (nm)	Interval of Kebab (nm)
3 h	10.3 ± 0.8	5.2 ± 0.3	15.8 ± 0.7
6 h	20.2 ± 1.1	5.4 ± 0.4	16.3 ± 1.0
12 h	22.4 ± 0.9	5.4 ± 0.4	15.5 ± 0.8

3.1.2. Morphologies of PE21M/RGO Rod-Like Crystals

We also investigate the effects of nanofillers with different dimensions on the crystallization behavior of PE21M. For the convenience of comparison, three crystallization temperatures (40, 50, and 60 °C) same as that of PE21M/SWCNT nanocomposites chosen to prepare PE21M/RGO nanocomposites. It can be seen from the crystals morphologies shown in Figure 3 that rod-like crystals were formed on the surface of RGO and the average sizes of PE21M crystals are listed in Table 3. Quite small particles with a size of 5.0 ± 0.2 nm can be observed on the surface of RGO nanosheets

at 40 °C, which grow into the largest lamellae with an average size of 18.0 ± 1.2 nm when the crystallization temperature increases to 50 °C. This suggests that PE21M chains need more time or much higher crystallization temperature to adjust their conformations to the surface of RGO. The size of PE21M lamellae formed on RGO is 16.0 ± 1.0 nm at 60 °C, smaller than that formed at 50 °C. It is obvious that the temperature dependence of the sizes of PE21M lamellae upon the RGO surface is similar the case observed in PE21M/SWCNT composites, namely, first it increases and then decreases with increasing crystallization temperature. It has been reported that the average sizes of lamellae formed on RGO become smaller and smaller with the increase of substituent bulk as the influence of substituent on crystal growth becomes more and more serious [36–38].

In this study, the smallest average size of lamellae is observed in PE21M/RGO composites, further verifying the conclusion that substituents have a great effect on crystal growth on RGO. We can also see from Table 3 that the thickness of rod-like crystals has the same variation rule with that of kebab crystals (Table 1), i.e., it increases with increasing crystallization temperature. Moreover, the thickness of crystals formed on SWCNTs and RGO under the same crystallization condition are almost the same by comparing the data in Tables 1 and 3. These findings all suggest that the isothermal crystallization temperature plays a decisive role in the thickness of lamellae formed on RGO. By comparison, the maximal thickness of PE21M lamellae formed on RGO is about 5.5 nm, which is much smaller than 8.8 nm of PE21F, 6.5 nm of PE21Cl, and 6.9 nm of PE21Br [36–38], which is also attributed to the influence of the largest methyl substituent. Obviously, PE21M crystals formed on RGO have much poorer regularity with respect to the cases in PE21F, PE21Cl, and PE21Br crystals [36–38] and hardly arrange at 60° directions apart from each other, which indicates that the largest substituent methyl significantly disturbs the matching between the molecular chain and RGO substrate. Furthermore, it is evident from Table 3 that the density (number/0.01 μm^2) of the lamellae decreases from eight at 50 °C to five at 60 °C, which is attributed to the less stable crystal nucleus existing at a lower undercooling degree. Meanwhile, the density of PE21X (X = F, Cl, Br, and CH_3) crystals prepared under the same supercooling degree decreases severely with the increase of the substituent's volume [36–38]. In other words, the maximum density of PE21M crystals formed on RGO is 8/0.01μm^2, much lower than 40/0.01 μm^2 of PE21F, 35/0.01 μm^2 of PE21Cl, and 37/0.01 μm^2 of PE21Br. Moreover, the density of PE21M crystals formed on RGO is significantly less than that formed on CNT comparing Figures 1 and 3. It is a generally accepted notion that lattice matching dominates the graphene-induced polymer epitaxial crystallization [19–22], which is of no concern for the "soft epitaxy" of CNTs [16–18]. Therefore, we can conclude that the lack of crystallographic mismatching is the main influencing factor that attaches the PE21M chain to the surface of RGO and after nucleation.
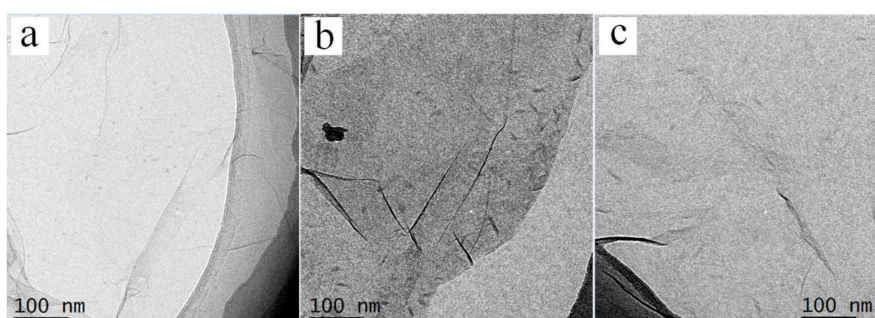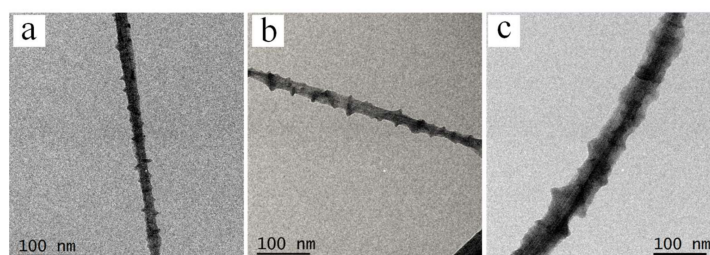

Figure 3. TEM images of PE21M/RGO nanocomposites produced in *p*-xylene at different temperatures for 6 h. (**a**) 40 °C, (**b**) 50 °C, and (**c**) 60 °C (both PE21Br and RGO concentrations are 0.05 wt %).

Table 3. The average size of PE21M lamella formed on RGO based on the TEM images of 200 lamellae.

Sample (Crystallization Temperature)	Size of Lamellae (nm)	Thickness of Lamellae (nm)	Density (number/0.01 μm^2)
PE21M/RGO (40 °C)	5.0 ± 0.2	3.0 ± 0.3	7.0
PE21M/RGO (50 °C)	18.0 ± 1.2	5.3 ± 0.4	8.0
PE21M/RGO (60 °C)	16.0 ± 1.0	5.5 ± 0.3	5.0

3.1.3. PE21M/Nanofiller Composites Prepared with the Assistance of Supercritical CO_2

Supercritical CO_2 (SC CO_2) was used to follow the antisolvent effect on PE21M crystallization. PE21M/nanofiller nanocomposites were prepared in *p*-xylene at 50 °C with the assistance of SC CO_2 and the experimental pressure of SC CO_2 was tuned to 10, 15, and 20 MPa. The crystallization morphologies are shown in Figures 4 and 5. SWCNTs are apt to agglomerate and form bundles under pressure of SC CO_2, which gradually becomes serious as the SC CO_2 pressures rises (Figure 4c). Therefore, the diameter of the SWCNTs are much thicker than that produced without SC CO_2 (Figure 1). The average sizes of the PE21M lamellae formed on SWCNTs and RGO are listed in Tables 4 and 5. After 3 h isothermal crystallization with the assistance of SC CO_2, the diameter of PE21M crystals formed on SWCNTs at 50 °C and 10 MPa, 23.5 ± 1.0 nm, is larger than that of crystals via solution isothermal crystallization after 6 h (20.2 ± 1.1 nm, Table 1). As the SC CO_2 pressure increases, the diameter of PE21M formed on SWCNTs at 15 MPa increases to 28.3 ± 1.1 nm. Similarly, the lamellae size of PE21M formed on RGO at 10 MPa, 20 ± 1.3 nm, is also larger than that of crystals formed without the assistance of SC CO_2 after 6 h of isothermal crystallization (Table 2). This suggests that SC CO_2 can accelerate the lateral growth of lamellae. The diameter of the PE21M kebab decreases with the increasing pressure of SC CO_2, from 28.3 ± 1.1 at 15 MPa to 20.5 ± 1.1 nm at 20 MPa. This phenomenon has also been observed previously [36–38], which can be attributed to the amount and speed of the PE21M molecular precipitation being greatly increased and the crystal growth being restrained at the excessively high CO_2 pressure. The interval of PE21M kebabs formed on SWCNTs becomes smaller due to the larger deposition of the PE21M chain, from 18.9 ± 0.8 nm at 10 MPa and 20.6 ± 0.9 nm at 15 MPa to 16.5 ± 0.8 nm at 20 MPa. For the crystallization of PE21M on RGO, the average sizes of the rod-like crystals of PE21M/RGO nanocomposites are about 20.0 ± 1.3, 28.0 ± 1.3, and 30.0 ± 1.5 nm, respectively, for 10, 15, and 20 MPa, which increase with the increasing pressure of SC CO_2. The density of the rod-like crystals has the same variation rule, i.e., increases from 11/0.01 μm^2 at 10 MPa and 15/0.01 μm^2 at 15 MPa to 18/0.01 μm^2 at 20 MPa. This fact indicates that the large deposition of molecular chains under SC CO_2 is beneficial to the attachment of PE21M on the surface of RGO, which then promotes the crystal growth. We can also find from Figures 4 and 5 and Tables 4 and 5 that the thicknesses of the crystal lamellae produced with the assistance of SC CO_2 are almost consistent with those prepared by traditional solution crystallization. This suggests that SC CO_2 can promote the lateral growth of lamellae on CNTs and RGO, but it cannot change the thickness of the crystal lamellae, which is directly related to crystallization temperature. There is an optimum SC CO_2 pressure of 15 MPa, at which the rod-like crystal lamellae size is the maximum.

Figure 4. TEM images of PE21M/SWCNT nanocomposites produced at different SC CO_2 pressures: (**a**) 10 MPa, (**b**) 15 MPa, and (**c**) 20 MPa in *p*-xylene at 50 °C for 3 h.

Table 4. The average size of PE21M lamellae formed on SWCNT with the assistance of SC CO_2 based on the TEM images of 200 lamellae.

| Sample (Pressure)	Diameter of Kebab (nm)	Thickness of Kebab (nm)	Interval of Kebab (nm)
PE21M/SWCNT (10 MPa)	23.5 ± 1.0	5.4 ± 0.6	18.9 ± 0.8
PE21M/SWCNT (15 MPa)	28.3 ± 1.1	5.5 ± 0.5	20.6 ± 0.9
PE21M/SWCNT (20 MPa)	20.5 ± 1.1	5.4 ± 0.7	16.5 ± 0.8
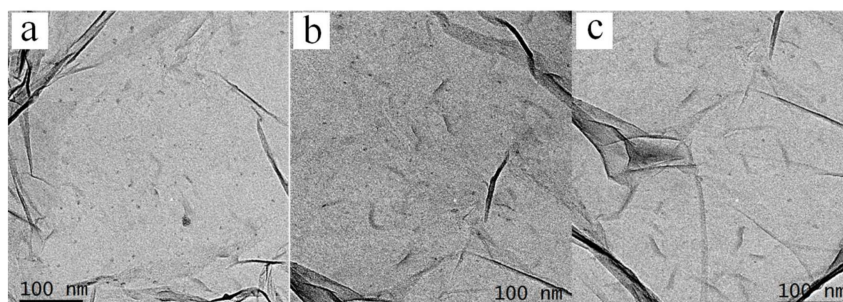
Figure 5. TEM images of PE21M/RGO nanocomposites produced at different SC CO_2 pressures: (**a**) 10 MPa, (**b**) 15 MPa, and (**c**) 20 MPa in *p*-xylene at 60 °C for 3 h.

Table 5. The average size of PE21M lamellae formed on RGO with assistance of SC CO_2 based on the TEM images of 200 lamellae.

Sample (Pressure)	Size of Lamellae (nm)	Thickness of Lamellae (nm)	Density (number/0.01 μm^2)
PE21M/RGO (10 MPa)	20.0 ± 1.3	5.4 ± 0.6	11
PE21M/RGO (15 MPa)	28.0 ± 1.3	5.6 ± 0.4	15
PE21M/RGO (20 MPa)	30.0 ± 1.5	5.6 ± 0.6	18

3.2. Thermal Behavior of PE21M/Nanofiller Composites

The melting behaviors of PE21M/nanofiller composites were measured by differential scanning calorimetry (DSC), as depicted in Figures 6 and 7. The melting peak temperatures of PE21M/nanofillers produced at 40 °C and 60 °C cannot be measured by DSC due to the very small size and quantity of epitaxial crystallized lamellae (Figures 1 and 3) and that of PE21M/nanofillers produced at 50 °C are 60.2 °C for PE21M/SWCNT and 60.5 °C for PE21M/RGO, which are all lower than that of PE21M (62.8 °C). This indicates that the thickness of lamellae formed on nanofillers is smaller than that of PE21M. We can also find from Table 6 that the melting temperature of PE21M/RGO nanocomposites is almost the same with that of PE21M/SWCNT under the same crystallization conditions, suggesting the analogical thickness of lamellae in both nanocomposites. The value of the heat of fusion (ΔH) of PE21M and nanocomposites are summarized in Table 6. The value of ΔH of PE21M/RGO composites is 0.16 J/g, much lower than 0.52 J/g of PE21M/CNT composites, which suggests that the quantity of crystals formed on RGO is much smaller than that formed on CNT.
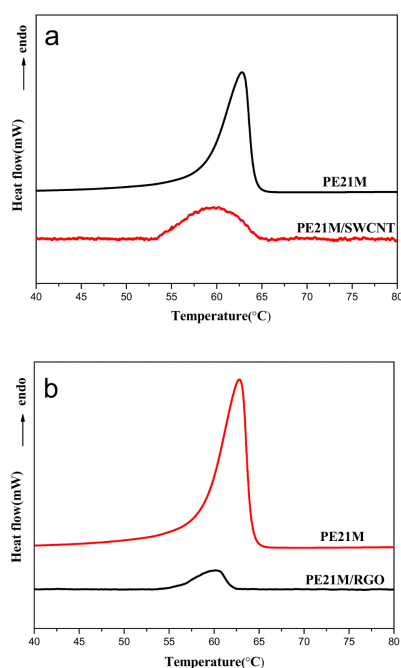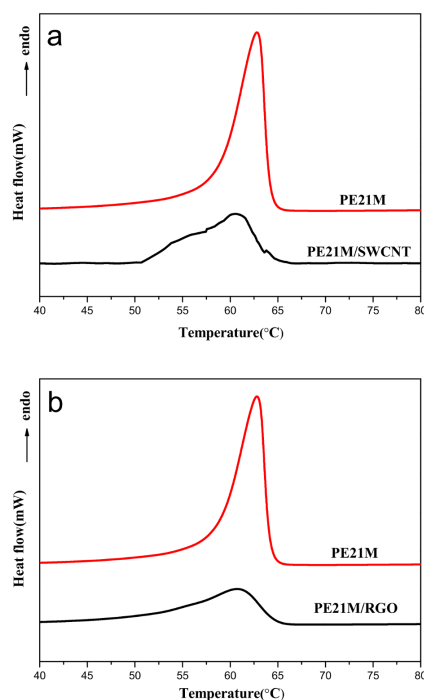
Figure 6. First heating curves of PE21M and PE21M/nanofiller composites in DSC measurement at a constant heating rate of 10 °C/min. (**a**) PE21M/SWCNT nanocomposites, and (**b**) PE21M/RGO nanocomposites.

Table 6. Melting data of PE21M and PE21M/nanofiller composites.

Sample	Tm (°C) Peak	Tm (°C) Onset	Onset-End (°C)	ΔH (J/g)
PE21M	62.8	58.0	6.8	18
PE21M/SWCNT	60.2	54.0	10.5	0.52
PE21M/RGO	60.5	56.2	5.7	0.16

PE21M/nanofiller composites produced at 50 °C and 15 MPa SC CO_2 pressure were taken as the example to investigate the influence of SC CO_2 on the melting behavior of PE21M crystals. We can find from Figure 6 and Table 7 that the melting peak temperature of PE21M/SWCNT nanocomposites produced at 50 °C is 60.5 °C for 15 MPa, which is almost consistent with that prepared by traditional solution crystallization (60.2 °C in Table 6). The same result is also observed in PE21M/RGO nanocomposites. The values of ΔH of PE21M/SWCNT and PE21M/RGO nanocomposites prepared at 50 °C and 15 MPa SC CO_2 pressure are 0.71 and 0.34 J/g, respectively, larger than that prepared by traditional solution crystallization (0.52 and 0.16 J/g shown in Table 6). This further suggests that supercritical CO_2 can promote the growth of lamellae on CNT and RGO, but the thickness of the crystal lamellae is directly related to crystallization temperature. The melting ranges of PE21M/SWCNT and PE21M/RGO nanocomposites prepared at 50 °C and 15 MPa SC CO_2 pressure are 13.5 and 12.2 °C, respectively, larger than that prepared by traditional solution crystallization (10.5 and 5.7 °C shown in Table 6). This is because the amount and speed of the PE21M precipitation from supercritical CO_2 is large, leading to the formation of more lamellae with inhomogeneous thickness.

Figure 7. First heating curves of PE21M and PE21M/nanofiller composites produced at 50 °C and 15 MPa SC CO_2 pressures in DSC measurement at a constant heating rate of 10 °C/min. (**a**) PE21M/SWCNT nanocomposites, and (**b**) PE21M/RGO nanocomposites.

Table 7. Melting data of PE21M and PE21M/nanofiller composites produced at 15 MPa SC CO_2 pressure.

Sample	Tm (°C) Peak	Tm (°C) Onset	Onset-End (°C)	ΔH (J/g)
PE21M	62.8	58.0	6.8	18
PE21M/SWCNT	60.5	50.7	13.5	0.71
PE21M/RGO	60.7	52.5	12.2	0.34

3.3. Crystalline Structure of PE21M/Nanofiller Composites

X-ray diffractograms of PE21M/nanofiller composites are exhibited in Figure 8 together with the patterns of PE21M and nanofillers. As shown in Figure 8a, two peaks centered at 19.4° and 22.2° in the XRD pattern can be observed, assigned to pure PE21M, indexed as (100) and (010) reflections of the triclinic cell [31]. For pristine nanofillers, the peak at 26.8° is assigned to the (002) reflection of carbon. Two peaks of 19.4° and 22.2° in PE21M/nanofiller composites are weak compared to virgin PE21M. This can be due to the fact that the quantity of epitaxial crystallized lamellae is small (Figures 1 and 3), which results in the weak diffracted intensities of (100) and (010) reflections. All the peaks for PE21M and nanofillers are found in the XRD pattern of PE21M/nanofiller composites without the obvious peak shift. This indicates that the nanofillers have quite a small influence on the crystal structure of PE21M. The XRD of PE21M/nanofiller composites prepared with the assistance of supercritical CO_2 (Supplementary Data Figures S2 and S3) again show the same results, further indicating that supercritical CO_2 cannot change the crystal structure of PE21M/nanofiller composites although it can effectively promote the growth of lamellae on CNT and RGO.
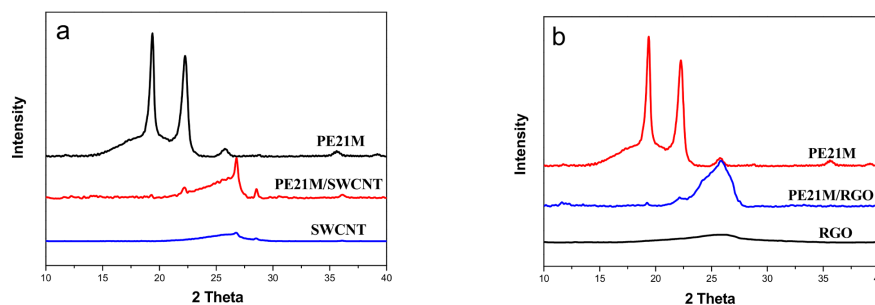
Figure 8. XRD diffractograms of PE21M, nanofillers, and PE21M/nanofiller composites. (**a**) PE21M/SWCNT nanocomposites, and (**b**) PE21M/RGO nanocomposites.

The substituent has a significant impact on the crystallization behavior of polyethylene since it acted as a defect of the chain to disturb the length of the continuous methylene sequences. This is confirmed by the fact that the orthorhombic lattice of PE21F is larger compared to that of HDPE, and the crystal lattice of PE21Cl and PE21Br are triclinic due to the accommodation of the bulky substituents [27,30]. Meanwhile, the melting temperatures of PE21F, PE21Cl, and PE21Br continuously decreased. With the substituent volume increasing in methyl (2 Å), the melting temperature of PE21M is much lower because of the lower-order triclinic form [27,30,31]. In our previous works [37,38], RGO could induce the structural transformation of PE21Cl and PE21Br from the triclinic form to the ordered orthorhombic form and generate extraordinary high melting temperatures due to the perfect lattice matching between polymers and RGO. SWCNT can only induce PE21Br to the orthorhombic form, and the melting temperatures of PE21Br/SWCNT nanocomposites are also lower than that of PE21Br/RGO nanocomposites because of the absent strict epitaxial crystallization. The results showed the capability that RGO induces substituted polymers to crystallize and generate an ordered chain packing structure because of the lattice matching. In this study, the triclinic lattice of PE21M cannot be changed by the induction of CNT and RGO. This suggests that the strong inductive effect from CNT and RGO cannot surmount the obstacle of methyl to the conformational adjustment of the PE21M molecular chain. Therefore, we conclude that polymers with the substituent volume greater than or equal to 2 Å (methyl) cannot be induced by CNT and graphene to form an ordered lattice structure. On the other hand, CNT and RGO show the different abilities that induce PE21M to nucleate, which can be explained by the different inducing mechanisms of both nanofillers. CNT induces the polymer to crystallize based on "soft epitaxy", that is, regardless of the lattice matching between the polymer chain and the graphitic sheet. Therefore, the number of the PE21M crystal nucleus formed on CNT was unaffected by the bulkier substituent, while, for two-dimensional RGO, the mechanism of RGO inducing the polymer is lattice matching, which will require adjusting the chain conformation to the surface of RGO. However, the bulky volume of methyl impedes the conformation adjustment of the PE21M chain, impacting the attachment of PE21M chain to the surface of RGO and nucleation. Consequently, the density of PE21M rod-like crystals formed on RGO is much smaller than that of kebab crystals on CNT.

4. Conclusions

The epitaxial crystallization behavior of PE21M on two different types of structural nanofillers, SWCNT and RGO, was investigated. The size and quantity of epitaxial crystallized lamellae formed on the surface of the nanofillers is small due to the bulkier substituent. The most suitable crystallization temperature for PE21M nanocomposites in *p*-xylene is 50 °C, at which the largest size and the most uniform lamellae of PE21M are formed. SC CO_2 can accelerate the growth of lamellae and improve the production of lamellae formed on nanofillers and the optimum SC CO_2 pressure for forming the maximum lamellae size is 15 MPa. The disparity in the density of crystals on CNT and RGO can be attributed to the different inducing mechanisms that show the different abilities of both nanofillers

to induce PE21M to nucleate. The triclinic crystal lattice structure and crystallizable sequence length of PE21M remain unchanged in the PE21M/nanofillers composite system. Therefore, the methyl is the threshold volume of the substituent that could be induced by nanofillers to form an ordered lattice structure. This study helps us infer whether substituted or branched polymers can be induced by carbonaceous nanofillers to crystallize and generate an ordered chain packing structure according to the volume of the substituent or branch. Meanwhile, it offers a referral to fabricate polymer-carbonaceous nanocomposites with a controllable chain packing structure and expected physical properties.

Supplementary Materials: The following are available online at http://www.mdpi.com/2073-4352/8/4/168/s1; **Figure S1**. ^{1}H NMR for (**A**) PE21M, (**B**) unsaturated polymer, and (**C**) monomer; **Figure S2**. XRD diffractograms of PE21M and PE21M/SWCNT composite produced at 50 °C and 15 MPa SC CO_2 pressure; **Figure S3**. XRD diffractograms of PE21M and PE21M/RGO composite produced at 50 °C and 15 MPa SC CO_2 pressure.

Author Contributions: This paper was accomplished based on the collaborative work of the authors. Weijun Miao performed the experiments, analyzed the data, interpreted the experimental results, and wrote the paper. Yiguo Li, Libin Jiang, Feng Wu, and Hao Zhu contributed to the experimental design. Hongbing Chen and Zongbao Wang supervised the entire research progress and analyzed the experimental results.

Conflicts of Interest: The authors declare no conflict of interest.

References

1. Wittmann, J.C.; Lotz, B. Epitaxial crystallization of polymers on organic and polymeric substrates. *Prog. Polym. Sci.* **1990**, *15*, 909–948. [CrossRef]

2. Chang, H.; Zhang, J.; Li, L.; Wang, Z.; Yang, C.; Takahashi, I.; Ozaki, Y.; Yan, S. A Study on the Epitaxial Ordering Process of the Polycaprolactone on the Highly Oriented Polyethylene Substrate. *Macromolecules* **2010**, *43*, 362–366. [CrossRef]

3. Wellinghoff, S.; Rybnikar, F.; Baer, E. Epitaxial crystallization of polyethylene. *J. Macromol. Sci. Phys.* **1974**, *10*, 1–39. [CrossRef]

4. Furuheim, K.M.; Axelson, D.E.; Antonsen, H.W.; Helle, T. Phase structural analyses of polyethylene extrusion coatings on high-density papers. I. Monoclinic crystallinity. *J. Appl. Polym. Sci.* **2010**, *91*, 218–225. [CrossRef]

5. Mittal, G.; Rhee, K.Y.; Park, S.J. The Effects of Cryomilling CNTs on the Thermal and Electrical Properties of CNT/PMMA Composites. *Polymers* **2016**, *8*, 169. [CrossRef]

6. Flores, A.; Poeppel, A.; Riekel, C.; Schulte, K. Evidence of a transcrystalline interphase in fiber PE homocomposites as revealed by microdiffraction experiments using synchrotron radiation. *J. Macromol. Sci. Phys.* **2001**, *40*, 749–761. [CrossRef]

7. Xu, J.Z.; Zhong, G.J.; Hsiao, B.S.; Fu, Q.; Li, Z.M. Low-dimensional carbonaceous nanofiller induced polymer crystallization. *Prog. Polym. Sci.* **2014**, *39*, 555–593. [CrossRef]

8. Yang, S.; Meng, D.; Sun, J.; Hou, W.; Ding, Y.; Jiang, S.; Huang, Y.; Geng, J. Enhanced electrochemical response for mercury ion detection based on poly(3-hexylthiophene) hybridized with multi-walled carbon nanotubes. *RSC Adv.* **2014**, *4*, 25051–25056. [CrossRef]

9. Xu, L.; Jiang, S.; Li, B.; Hou, W.; Li, G.; Memon, M.A.; Huang, Y.; Geng, J. Graphene Oxide: A Versatile Agent for Polyimide Foams with Improved Foaming Capability and Enhanced Flexibility. *Chem. Mater.* **2015**, *27*, 4358–4367. [CrossRef]

10. Zhu, W.; Yang, O.; Sun, J.; Memon, J.; Wang, C.; Geng, J.; Huang, Y. Scalable preparation of three-dimensional porous structures of reduced graphene oxide/cellulose composites and their application in supercapacitors. *Carbon* **2013**, *62*, 501–509.

11. Ning, N.; Fu, S.; Zhang, W.; Chen, F.; Wang, K.; Deng, H.; Zhang, Q.; Fu, Q. Metal-catalyst-free growth of carbon nanotubes/carbon nanofibers on carbon blacks using chemical vapor deposition. *Prog. Polym. Sci.* **2012**, *37*, 1425–1455. [CrossRef]

12. Mai, F.; Wang, K.; Yao, M.; Deng, H.; Chen, F.; Fu, Q. Superior Reinforcement in Melt-Spun Polyethylene/Multiwalled Carbon Nanotube Fiber through Formation of a Shish-Kebab Structure. *J. Phys. Chem. B* **2010**, *114*, 10693–10702. [CrossRef] [PubMed]

13. Li, A.; Zhang, C.; Zhang, Y.F. Thermal Conductivity of Graphene-Polymer Composites: Mechanisms, Properties, and Applications. *Polymers* **2017**, *9*, 437–454.

14. Deng, H.; Skipa, T.; Zhang, R.; Lellinger, D.; Bilotti, E.; Alig, I.; Peijs, T. Effect of melting and crystallization on the conductive network in conductive polymer composites. *Polymer* **2009**, *50*, 3747–3754. [CrossRef]

15. Deng, H.; Skipa, T.; Bilotti, E.; Zhang, R.; Lellinger, D.; Mezzo, L.; Fu, Q.; Alig, I.; Peijs, T. Preparation of High-Performance Conductive Polymer Fibers through Morphological Control of Networks Formed by Nanofillers. *Adv. Funct. Mater.* **2010**, *20*, 1424–1432. [CrossRef]

16. Kodjie, S.L.; Li, L.; Li, B.; Cai, W.; Li, C.Y.; Keating, M. Morphology and Crystallization Behavior of HDPE/CNT Nanocomposite. *J. Macromol. Sci. Phys.* **2006**, *45*, 231–245. [CrossRef]

17. Li, C.Y.; Li, L.; Cai, W.; Kodjie, S.L.; Tenneti, K.K. Nano hybrid shish-kebab: Periodically functionalize carbon nanotubes. *Adv. Mater.* **2005**, *17*, 1198–1202. [CrossRef]

18. Li, L.; Li, C.Y.; Ni, C. Polymer Crystallization-Driven, Periodic Patterning on Carbon Nanotubes. *J. Am. Chem. Soc.* **2006**, *128*, 1692–1699. [CrossRef] [PubMed]

19. Tracz, A.; Jeszka, J.K.; Kucinska, I.; Chapel, J.P.; Boiteux, G.; Kryszewski, M. Influence of the crystallization conditions on the morphology of the contact layer of polyethylene crystallized on graphite: Atomic force microscopy studies. *J. Appl. Polym. Sci.* **2002**, *86*, 1329–1336. [CrossRef]

20. Tracz, A.; Kucinska, I.; Jeszka, J.K. Formation of Highly Ordered, Unusually Broad Polyethylene Lamellae in Contact with Atomically Flat Solid Surfaces. *Macromolecules* **2003**, *36*, 10130–10132. [CrossRef]

21. Tracz, A.; Kucinska, I.; Jeszka, J.K. Unusual crystallization of polyethylene at melt/atomically flat interface: Lamellar thickening growth under normal pressure. *Polymer* **2006**, *47*, 7251–7258. [CrossRef]

22. Takenaka, Y.; Miyaji, H.; Hoshino, A.; Tracz, A.; Jeszka, J.K.; Kucinska, I. Interface Structure of Epitaxial Polyethylene Crystal Grown on HOPG and MoS_2 Substrates. *Macromolecules* **2004**, *37*, 9667–9669. [CrossRef]

23. Vadlamudi, M.; Alamo, R.G.; Fiscus, D.M.; Varma-Nair, M.J. Inter and intra-molecular branching distribution of tailored LLDPEs inferred by melting and crystallization behavior of narrow fractions. *J. Therm. Anal. Calorim.* **2009**, *96*, 697–704. [CrossRef]

24. Vadlamudi, M.; Subramanian, G.; Shanbhag, S.; Alamo, R.G.; Fiscus, D.M.; Brown, G.M.; Lu, C.; Ruff, C.J. Molecular Weight and Branching Distribution of a High Performance Metallocene Ethylene 1-Hexene Copolymer Film-Grade Resin. *Macromol. Symp.* **2009**, *282*, 1–13. [CrossRef]

25. Smith, J.A.; Brzezinska, K.R.; Valenti, D.J.; Wagener, K.B. Precisely Controlled Methyl Branching in Polyethylene via Acyclic Diene Metathesis (ADMET) Polymerization. *Macromolecules* **2000**, *33*, 3781–3794. [CrossRef]

26. Sworen, J.C.; Smith, J.A.; Berg, J.M.; Wagener, K.B. Modeling Branched Polyethylene: Copolymers Possessing Precisely Placed Ethyl Branches. *J. Am. Chem. Soc.* **2004**, *126*, 11238–11246. [CrossRef] [PubMed]

27. Boz, E.; Wagener, K.B.; Ghosal, A.; Fu, R.; Alamo, R.G. Synthesis and Crystallization of Precision ADMET Polyolefins Containing Halogens. *Macromolecules* **2006**, *39*, 4437–4447. [CrossRef]

28. Sworen, J.C.; Wagener, K.B. Linear Low-Density Polyethylene Containing Precisely Placed Hexyl Branches. *Macromolecules* **2007**, *40*, 4414–4423. [CrossRef]

29. Boz, E.; Ghiviriga, I.; Nemeth, A.J.; Jeon, K.; Alamo, R.G.; Wagener, K.B. Random, Defect-Free Ethylene/Vinyl Halide Model Copolymers via Condensation Polymerization. *Macromolecules* **2008**, *41*, 25–30. [CrossRef]

30. Boz, E.; Nemeth, A.J.; Wagener, K.B.; Jeon, K.; Smith, R.; Nazirov, F.; Bockstaller, M.R.; Alamo, R.G. Well-Defined Precision Ethylene/Vinyl Fluoride Polymers: Synthesis and Crystalline Properties. *Macromolecules* **2008**, *41*, 1647–1653. [CrossRef]

31. Rojas, G.; Inci, B.; Wei, Y.; Wagener, K.B. Precision polyethylene: Changes in morphology as a function of alkyl branch size. *J. Am. Chem. Soc.* **2009**, *131*, 17376–17386. [CrossRef] [PubMed]

32. Inci, B.; Lieberwirth, I.; Steffen, W.; Mezger, M.; Graf, R.; Landfester, K.; Wagener, K.B. Decreasing the Alkyl Branch Frequency in Precision Polyethylene: Effect of Alkyl Branch Size on Nanoscale Morphology. *Macromolecules* **2012**, *45*, 3367–3376. [CrossRef]

33. Gaines, T.W.; Nakano, T.; Chujo, Y.; Trigg, E.B.; Winey, K.I.; Wagener, K.B. Precise Sulfite Functionalization of Polyolefins via ADMET Polymerization. *ACS Macro Lett.* **2015**, *4*, 624–627. [CrossRef]

34. Tasaki, M.; Yamamoto, H.; Hanesaka, M.; Tashiro, K.; Boz, E.; Wagener, K.B.; Ruiz-Orta, C.; Alamo, R.G. Polymorphism and Phase Transitions of Precisely Halogen-Substituted Polyethylene. (1) Crystal Structures of Various Crystalline Modifications of Bromine-Substituted Polyethylene on Every 21st Backbone Carbon. *Macromolecules* **2014**, *47*, 4738–4749. [CrossRef]

35. Kaner, P.; Ruiz-Orta, C.; Boz, E.; Wagener, K.B.; Tasaki, M.; Tashiro, K.; Alamo, R.G. Kinetic Control of Chlorine Packing in Crystals of a Precisely Substituted Polyethylene. Toward Advanced Polyolefin Materials. *Macromolecules* **2014**, *47*, 236–245. [CrossRef]

36. Miao, W.; Lv, Y.; Zheng, W.; Wang, Z.; Chen, Z.R. Epitaxial crystallization of precisely fluorine substituted polyethylene induced by carbon nanotube and reduced graphene oxide. *Polymer* **2016**, *83*, 205–213. [CrossRef]

37. Miao, W.; Wang, Z.; Li, Z.; Zheng, W.; Chen, Z.R. Epitaxial crystallization of precisely chlorine-substituted polyethylene induced by carbon nanotube and graphene. *Polymer* **2016**, *94*, 53–61. [CrossRef]

38. Miao, W.; Wang, B.; Li, Y.; Zheng, W.; Chen, H.; Zhang, L.; Wang, Z. Epitaxial crystallization of precisely brominesubstituted polyethylene induced by carbon nanotubes and graphene. *RSC Adv.* **2017**, *7*, 17640–17649. [CrossRef]

39. Wang, B.; Li, H.; Li, Z.; Chen, P.; Wang, Z.; Gu, Q. Electrostatic adsorption method for preparing electrically conducting ultrahigh molecular weight polyethylene/graphene nanosheets composites with a segregated network. *Compos. Sci. Technol.* **2013**, *89*, 180–185. [CrossRef]

40. Zhang, Z.; Xu, Q.; Chen, Z.; Yue, Z. Nanohybrid Shish-Kebabs: Supercritical CO_2-Induced PE Epitaxy on Carbon Nanotubes. *Macromolecules* **2008**, *41*, 2868–2873. [CrossRef]